



ELSEVIER

Available online at www.sciencedirect.com

Experimental Neurology xx (2008) xxx–xxx

**Experimental  
Neurology**

www.elsevier.com/locate/yexnr

## Mitochondrial fusion and function in Charcot–Marie–Tooth type 2A patient fibroblasts with mitofusin 2 mutations

Elizabeth A. Amriott<sup>a</sup>, Paul Lott<sup>b,1</sup>, Jamie Soto<sup>c</sup>, Peter B. Kang<sup>d</sup>, J. Michael McCaffery<sup>e</sup>,  
Salvatore DiMauro<sup>f</sup>, E. Dale Abel<sup>c</sup>, Kevin M. Flanigan<sup>b</sup>,  
Victoria H. Lawson<sup>b,\*,2</sup>, Janet M. Shaw<sup>a,\*</sup>

<sup>a</sup> Department of Biochemistry, University of Utah School of Medicine, Salt Lake City, UT, 84112, USA

<sup>b</sup> Departments of Neurology, Human Genetics, Pathology, and Pediatrics, University of Utah School of Medicine, Salt Lake City, UT 84112, USA

<sup>c</sup> Division of Endocrinology Metabolism and Diabetes and Program in Human Molecular Biology and Genetics, University of Utah, School of Medicine, Salt Lake City, UT 84112, USA

<sup>d</sup> Department of Neurology, Children's Hospital Boston and Harvard Medical School, Boston, MA 02115, USA

<sup>e</sup> Integrated Imaging Center, Department of Biology, Johns Hopkins University, Baltimore, MD 21218, USA

<sup>f</sup> Department of Neurology, Columbia University Medical Center, New York, NY 10032, USA

Received 5 November 2007; revised 6 January 2008; accepted 11 January 2008

### Abstract

Charcot–Marie–Tooth Type 2A is a dominantly inherited peripheral neuropathy characterized by axonal degeneration of sensory and motor nerves. The disease is caused by mutations in the mitochondrial fusion gene *MFN2*. *Mfn2* is an integral outer mitochondrial membrane protein composed of a large GTPase domain and two heptad repeat (HR) domains that face the cytoplasm. Mitochondrial membrane fusion and division are balanced processes that are necessary to maintain tubular mitochondrial morphology, respiratory function, and uniform distribution of the organelle throughout the cell. We have utilized primary fibroblasts from CMT2A patients to survey mitochondrial phenotypes associated with heterozygous *MFN2* alleles expressed at physiological levels. Our results indicate that, in fibroblasts, mitofusin expression, mitochondrial morphology, ultrastructure, mtDNA content, and respiratory capacity are not affected by the presence of mutant *Mfn2* protein. Consistent with a lack of mitochondrial dysfunction, we also show that mitochondrial fusion occurs efficiently in CMT2A patient-derived fibroblasts. Our observations are in agreement with the neuronal specificity of the disease and are consistent with a recent finding that mitochondrial fusion can be maintained in cells that express mutant *Mfn2* protein due to complementation by a second mitofusin, *Mfn1*. We discuss our results and those of others in terms of a comprehensive model for the mechanism(s) by which mutations in *MFN2* may lead to CMT2A disease.

© 2008 Published by Elsevier Inc.

**Keywords:** CMT2A; Peripheral neuropathy; Mitochondria; Mitofusin; *Mfn2*; *Mfn1*; GTPase; Membrane fusion; Fibroblasts

### Introduction

In the past decade it has become increasingly clear that the regulation of mitochondrial dynamics, including fusion, division, and transport, is vital to cell viability, particularly in cells with very high energetic demands such as neurons (reviewed by (Baloh, 2007, Chan, 2006a, Chan, 2007, Chen and Chan, 2006) Charcot–Marie–Tooth disease Type 2A (CMT2A) is an autosomal dominant axonal peripheral neuropathy caused by heterozygous mutations in *MFN2*, the gene encoding Mitofusin 2 (*Mfn2*) (Chung et al., 2006, Kijima et al., 2005, Lawson et al.,

\* Corresponding authors. J.M. Shaw is to be contacted at University of Utah; School of Medicine, Department of Biochemistry, 15 N Medical Drive East, Rm 4100, Salt Lake City, UT 84112, USA. Fax: +1 801 591 7959. V.H. Lawson is to be contacted at The Ohio State University, Division of Neuromuscular Diseases, Department of Neurology, 461 Means Hall, 1654 Upham Drive, Columbus, OH 43210, USA. Fax: +1 614 293 6111.

E-mail addresses: Victoria.Lawson@osumc.edu (V.H. Lawson), shaw@biochem.utah.edu (J.M. Shaw).

<sup>1</sup> Current address: Genome Center, Section of Molecular Biology, Division of Biological Sciences, University of California at Davis, Davis, CA 95616, USA.

<sup>2</sup> Current address: Division of Neuromuscular Diseases, Department of Neurology, The Ohio State University, Columbus, OH 43210, USA.

0014-4886/\$ - see front matter © 2008 Published by Elsevier Inc.  
doi:10.1016/j.expneurol.2008.01.010

2005, Verhoeven et al., 2006, Zuchner et al., 2006, Zuchner et al., 2004). Mfn2 is one of two mitofusin proteins that are directly involved in the regulated fusion of mitochondrial membranes and in the maintenance of tubular mitochondrial morphology (Eura et al., 2003, Ishihara et al., 2004, Legros et al., 2002, Santel et al., 2003). Mfn1 and Mfn2 are conserved integral outer mitochondrial membrane proteins, each consisting of a large GTPase domain and two heptad repeat (HR), or putative coiled-coil domains, all of which face the cytoplasm (reviewed by (Chan, 2006b, Okamoto and Shaw, 2005)). Mouse knockout studies have shown that loss of either Mfn1 (*MFN1*<sup>-/-</sup>) or Mfn2 (*MFN2*<sup>-/-</sup>) is embryonic lethal, and double mitofusin knockout mouse embryonic fibroblasts (MEFs) exhibit severely fragmented mitochondria, slow growth, altered mitochondrial membrane potential, and decreased respiratory activity (Chen et al., 2005, Chen et al., 2003). Mitochondrial fusion has been proposed to promote and preserve the “health” and functionality of this essential organelle via the regular inter-mixing of matrix contents, including mitochondrial DNA (mtDNA) (Chan, 2006b, Chen and Chan, 2006, Detmer and Chan, 2007b).

CMT2A causes progressive length-dependent sensory loss, distal muscle atrophy and weakness, and foot deformities in patients with *MFN2* mutations (Lawson et al., 2005, Zuchner et al., 2006, Zuchner et al., 2004). Reduced compound motor action potential amplitudes indicate that symptoms result from axonal loss or degeneration in peripheral nerves (Chung et al., 2006, Lawson et al., 2005, Verhoeven et al., 2006). In addition to CMT2A, mutations in *MFN2* have recently been identified in patients with HMSN VI, another CMT-related peripheral neuropathy with optic atrophy (Verhoeven et al., 2006, Zuchner et al., 2006). Similarly, mutations in the mitochondrial fusion gene *OPA1* cause Dominant Optic Atrophy (DOA) (Delettre et al., 2000) and some cases of CMT4A are caused by mutations in *GDAP1* (Baxter et al., 2002, Cuesta et al., 2002), a mitochondrial outer membrane protein with a putative role in mitochondrial division (Niemann et al., 2005). This growing collection of neuropathies associated with mutant mitochondrial proteins highlights the significant contribution of mitochondrial dynamics to neurological function.

Studies in cells expressing CMT2A-associated *MFN2* alleles have suggested models for the molecular basis and the neuronal specificity of the disease. In one study, overexpression of mutant *MFN2* in primary rat dorsal root ganglion (DRG) cells resulted in the accumulation of mitochondria in the cell body, fewer mitochondria in distal axons, and an increased number of stationary organelles (Baloh et al., 2007). The authors proposed that CMT2A alleles impair mitochondrial transport, leading to specific degeneration in the highly polar and lengthy axons of peripheral nerves. An alternative model was based on the expression of CMT2A-causing *MFN2* alleles in single and double mitofusin knockout MEFs (Detmer and Chan, 2007a). This analysis revealed that Mfn1 can functionally complement the fusion defect of several mutant *MFN2* alleles. Hence, lower Mfn1 expression levels in neurons could explain the neuronal specific consequences of CMT2A-associated mutations. Finally, mitochondrial function was examined in fibroblasts obtained from four CMT2A patients carrying three of the

approximately 40 known *MFN2* mutations (Loiseau et al., 99 2007). Mitochondria in these patient fibroblasts formed normal 100 tubular networks but displayed an energetic coupling defect, 101 which could contribute to the axonal degeneration observed in 102 CMT2A patients. Thus, despite what is known about the role of 103 Mfn2 in mitochondrial fusion, the molecular pathogenesis of 104 *MFN2* mutations in CMT2A remains unclear. 105

Although the pathological effects of CMT2A alleles would ideally be evaluated in CMT2A patient-derived neurons, these 106 tissues are not readily available. However, primary patient 107 fibroblasts can be easily acquired and have practical advantages 108 over studies in knockout mice and in neuronal culture systems. In 109 particular, methods for studying mitochondrial fusion are well 110 established in fibroblasts (Chen et al., 2005, Chen et al., 2003), 111 and patient cells allow the evaluation of mutant alleles at native 112 expression levels, thereby avoiding phenotypes caused by Mfn2 113 overexpression (Detmer and Chan, 2007a, Eura et al., 2003, 114 Huang et al., 2007, Rojo et al., 2002). In this study, we char- 115 acterized mitochondrial fusion and function in cultured primary 116 fibroblasts obtained from five CMT2A patients with distinct 117 *MFN2* mutations. Fibroblasts were evaluated for changes in 118 Mfn2 and Mfn1 protein abundance, mitochondrial morphology, 119 mtDNA integrity, respiratory function, and membrane fusion. We 120 found that mitochondrial dynamics and function were preserved 121 in patient fibroblasts endogenously expressing both wild-type 122 (WT) and mutant Mfn2 proteins, as well as Mfn1. This estab- 123 lishes that heterozygous *MFN2* mutations are not sufficient to 124 disrupt mitochondrial fusion or alter mitochondrial function in 125 fibroblasts. These results are consistent with the neuronal 126 specificity of CMT2A and establish that patient fibroblasts are 127 not the preferred experimental system for determining the path- 128 ogenic mechanism of the disease. On the other hand, patient 129 fibroblasts may provide a useful system for studying the com- 130 pensating mechanisms that protect most CMT2A patient tissues. 131 132

## Materials and methods 133

### Cell culture 134

Patients with Charcot–Marie–Tooth Type 2A (CMT2A) 135 caused by three different point mutations in Mfn2 (T105M, 136 I213T, and V273G) have been described previously (Lawson 137 et al., 2005). The clinical descriptions of two additional CMT2A 138 patients carrying novel *MFN2* mutations, located in the GTPase 139 (F240I) and HR2 (L734V) domains of the protein will be pre- 140 sented elsewhere. Under an IRB approved protocol, and fol- 141 lowing informed consent, skin punches were obtained from 142 CMT2A patients harboring the mutations cited above. Primary 143 fibroblast cultures were established using standard cell culture 144 procedures. A skin punch was also obtained from an unrelated, 145 unaffected individual with WT *MFN2*. Cultured fibroblasts from 146 the normal individual were used throughout this work as the 147 Control sample. Under standard culture conditions (low glucose 148 Dulbecco’s Modified Eagle’s Medium (Invitrogen) supple- 149 mented with 10% Fetal Bovine Serum (Hyclone) incubated at 150 37 °C with 5% CO<sub>2</sub>) the CMT2A patient-derived fibroblasts 151 exhibited cellular morphology and growth characteristics similar 152

153 to those of the Control culture and could be maintained for  
154 approximately 15 passages (P15). All experiments were per-  
155 formed on early to mid-passage cells (P4–P9) unless otherwise  
156 indicated.

#### 157 *Mitofusin protein analysis*

158 Total cellular protein was prepared from  $1 \times 10^6$  cells lysed  
159 with Cell Disruption Buffer (Ambion). 10  $\mu$ g total protein per  
160 sample was separated by electrophoresis on an 8% polyacry-  
161 lamide-SDS gel. Separated proteins were transferred to  
162 nitrocellulose and specific proteins were detected by immuno-  
163 decoration with anti-Mfn2 (1/1000 dilution; Sigma #M6444),  
164 anti-porin (1/10,000 dilution; Molecular Probes #A31855), and  
165 anti-Mfn1 (1/250 dilution, a generous gift from M. Rojo). HRP-  
166 conjugated mouse or rabbit secondary antibodies were detected  
167 by ECL illumination (ECL Plus Western Blotting Reagent, GE  
168 LifeSciences) and densitometric analysis of the resulting films  
169 was used to quantify the signal of each protein band (Quantity  
170 One, Bio-Rad). The ratio of Mfn2 to porin was determined for  
171 each sample and all CMT2A samples were normalized to the  
172 Control sample (Control = 1.00;  $n = 3$ ).

173 For sub-cellular fractionation, cells were harvested, resus-  
174 pended in Homogenization Buffer (250 mM Sucrose, 20 mM  
175 Tris, pH7.4, 140 mM NaCl, 10 mM KCl, 1.5 mM MgCl<sub>2</sub>, 1 mM  
176 DTT, 1 $\times$  Complete EDTA-free protease inhibitor cocktail  
177 (Roche)) and disrupted in a dounce homogenizer. Homogenates  
178 were centrifuged at 800  $\times g$  to pellet nuclei and unlysed cells. The  
179 resulting supernatant was spun for 15 min at 10,000  $\times g$  to  
180 generate mitochondrial pellet (Mito) and post-mitochondrial  
181 supernatant (PMS) fractions. 5  $\mu$ g protein from each fraction was  
182 separated by electrophoresis as described above and samples  
183 were analyzed for the presence of Mfn2, porin, and GAPDH (1/  
184 10,000 dilution; Sigma #G8795) by standard Western procedures.

#### 185 *MitoTracker staining and fluorescence microscopy*

186 Approximately 10,000 cells per population were plated on  
187 35 mm poly-D-lysine coated glass-bottom culture dishes  
188 (MatTek Corp.) in standard medium and incubated at 37  $^{\circ}$ C  
189 for at least 24 h. For mitochondrial staining, standard medium  
190 was replaced with medium containing 15nM MitoTracker<sup>®</sup> Red  
191 CM-H<sub>2</sub>XROS (Molecular Probes) and cells were incubated  
192 with the dye at 37  $^{\circ}$ C for 6–8 h. After incubation, cells were  
193 washed twice with Phosphate Buffered Saline. Mitochondria in  
194 live cells were visualized by fluorescence microscopy and  
195 mitochondrial morphology was scored as either Tubular,  
196 Mixed, or Fragmented. Images were obtained by standard or  
197 confocal fluorescence microscopy (Olympus IX71 or Olympus  
198 IX81 confocal, University of Utah School of Medicine Cell  
199 Imaging Facility).

#### 200 *Electron microscopy*

201 Mitochondrial morphology and ultrastructure were evaluated  
202 by transmission electron microscopy. Low passage (P3–P6)  
203 fibroblast cultures were grown to 70–80% confluence in stan-

dard 10 cm culture dishes as described above. Cells were fixed 204  
for 1 h at room temperature (3.0% formaldehyde, 1.5% gluta- 205  
raldehyde in 0.1 M NaCacodylate, 5 mM Ca<sup>2+</sup>, 2.5% sucrose, 206  
pH 7.4) and washed three times (15 min per wash; 0.1 M 207  
NaCacodylate, 2.5% sucrose, pH 7.4). Cells were processed, 208  
sectioned, and analyzed as described previously (McCaffery 209  
and Farquhar, 1995). Briefly, cells were post-fixed in Palade's 210  
OsO<sub>4</sub>, stained in Kellenberger's uranyl acetate, dehydrated and 211  
embedded in epon for sectioning. Images were collected on a 212  
Phillipis EM 410 TEM equipped with a Soft Imaging System 213  
Megaview III digital camera. 214

#### 215 *Mitochondrial DNA analysis*

216 PCR analysis for detection of large-scale mitochondrial 216  
deletions was performed essentially as described previously 217  
(Kleinle et al., 1997) except that the primers were used in 218  
different combinations to generate products for two distinct 219  
regions of the genome. Briefly, genomic DNA was isolated 220  
either from snap-frozen muscle biopsy samples or  $\sim 1 \times 10^7$  P5 221  
and P11 Control and CMT2A patient-derived fibroblasts. 222  
DNA isolated from muscle of individuals with Kearns–Sayre 223  
Syndrome (KSS) or Chronic Progressive External Opthamol- 224  
plegia (CPEO) served as positive controls for single (KSS) and 225  
multiple (CPEO) mtDNA deletions. PCR amplification was 226  
performed using the Expand Long Template PCR System 227  
(Roche), with 100 ng template DNA and 300 nM primers 228  
D1B/OLA or D1A/OLB (Kleinle et al., 1997). Primer pair 229  
D1B/OLA generates an  $\sim 11$  kb product that extends from the 230  
heavy strand origin of replication (O<sub>H</sub>) to the light strand 231  
origin (O<sub>L</sub>). This region of the genome is commonly deleted or 232  
rearranged in mitochondrial disorders. Primer pair D1A/OLB 233  
generates an  $\sim 5.6$  kb product that covers a region from O<sub>L</sub> to 234  
O<sub>H</sub>, where deletions are rare. Together, the two reactions cover 235  
the entire mitochondrial genome. PCR products were separated 236  
on a 1% agarose gel and visualized by staining with ethidium 237  
bromide. 238

239 Mitochondrial and nuclear DNA quantification was per- 239  
formed by quantitative real-time PCR (qRT-PCR) (Higuchi 240  
et al., 1993), using a protocol similar to that reported previously 241  
for measuring quantities of telomeric DNA relative to nuclear 242  
DNA (Cawthon, 2002). Total cellular DNA was extracted from 243  
fibroblasts using the DNeasy Blood and Tissue Kit (Qiagen) and 244  
DNA yield was determined using the ND-1000 Spectro- 245  
photometer (NanoDrop). The single-copy nuclear gene  $\beta$ -globin 246  
and a region of mtDNA from bp 3130 to bp 3301 were amplified 247  
from 20 ng total input DNA in separate 25  $\mu$ l real-time PCR 248  
reactions. The primers used to amplify mtDNA were previously 249  
shown to be specific for mtDNA and do not co-amplify nuclear 250  
sequences (Parfait et al., 1998). Each template was mixed with 251  
Power SYBR<sup>®</sup> Green PCR Master Mix (Applied Biosystems) 252  
and 200 nM primers (Integrated DNA Technologies, Inc.). 253  
Cycling and real-time detection was performed with the ABI 254  
PRISM<sup>®</sup> 7900 Sequence Detection System. Cycling conditions 255  
were as follows: 50  $^{\circ}$ C for 2 min, 95  $^{\circ}$ C for 10 min, followed by 256  
35 cycles of 95  $^{\circ}$ C for 30 s, 50  $^{\circ}$ C for 45 s, 72  $^{\circ}$ C for 30 s. A 257  
dissociation profile was run on each sample and negative (no 258

template) controls to confirm SYBR Green fluorescence detection was specific for the desired amplification product. In each experiment, 5 ng–40 ng total DNA from the Control sample was amplified with both sets of primers to generate standard curves for quantification of the test samples. Using Cycle Threshold (Ct) values, the quantity of mtDNA and  $\beta$ -globin was determined from the corresponding standard curve (SDS 2.1.1 analysis software, Applied Biosystems) (See Supplemental Table 1) and relative amounts of mtDNA in each sample were calculated as the ratio of mtDNA to  $\beta$ -globin. All samples were amplified in quadruplicate in each experiment and the experiment was performed in triplicate. Statistical analyses were performed using PRISM<sup>®</sup> analytical software (GraphPad, Inc.) or Excel (Microsoft, Inc.).

### 273 Respiration measurements

274 Basal and maximal (uncoupled) respiration rates were determined for individual fibroblast populations (Control, T105M, I213T, and V273G) by measuring oxygen consumption with a fiber-optic oxygen sensing probe (Ocean Optics, Denudin, FL) essentially as described previously (Chen et al., 2005, O'Neill et al., 2007). Briefly,  $8 \times 10^6$  cells were suspended in 2 mL Buffer TD (137 mM NaCl, 5 mM KCl, 0.7 mM Na<sub>2</sub>HPO<sub>4</sub>, 25 mM Tris–Cl, pH 7.4) and transferred to the oxygen chamber. Following one minute of mixing to equilibrate the sample, the chamber was stoppered and allowed to equilibrate for an additional 2 min. Endogenous (basal) respiration was measured for 1 min. The uncoupler 2,4-dinitrophenol (DNP) was injected into the chamber (83 mM final) at 4.5 min after stoppering. Maximal (uncoupled) respiration was measured for 1 min starting 0.5 min after the DNP injection.

289 Respiratory complex enzyme activities were measured from Control and three mutant fibroblast cultures (T105M, I213T, and V273G) as described previously (DiMauro et al., 1987). Enzyme activity was calculated as nmol/min/mg protein normalized to the mitochondrial matrix protein citrate synthase (CS).

### 295 PEG fusion assay

296 Plasmids pAC-GFP-mito (mito-GFP) and pDsRed2-mito (mito-RFP) (Clontech) were introduced into primary fibroblasts using the Amaxa Nucleofection System (Amaxa Biosystems, Germany) according to the manufacturer's protocol for primary fibroblasts. 48 h post-nucleofection nearly 90% of each culture expressed the appropriate mitochondrially targeted fluorophore. Fibroblasts expressing mito-GFP and mito-RFP were co-cultured (~15,000 cells each) overnight in poly-D-lysine treated 4-well slide chambers and the polyethylene glycol (PEG) fusion assay was performed essentially as described (Chen et al., 2005, Chen et al., 2003). Nine hours after PEG/cycloheximide treatment, cell hybrids were permeabilized and stained with DAPI, then fixed with 3.7% formaldehyde and treated with ProLong Gold<sup>®</sup> antifade reagent (Molecular Probes). Cell hybrids were visually evaluated for mitochondrial fusion and images were obtained by confocal

fluorescence microscopy (Olympus IX81, University of Utah School of Medicine Cell Imaging Facility). Previous studies have established that PEG treatment alone does not induce mitochondrial membrane fusion (Chen et al., 2005, Chen et al., 2003, Eura et al., 2003, Koshiba et al., 2004, Mattenberger et al., 2003).

## Results

### *Mutant Mfn2 proteins are properly expressed and localized to mitochondria*

Although CMT2A patients are heterozygous for *MFN2* mutations, it is not known whether the CMT2A disease phenotype results from mitofusin insufficiency or dominant-negative disruption of mitofusin function. *MFN2* mutations could produce haploinsufficiency as a result of either loss-of-function of the intact mutant protein or altered expression, stability, or localization of the mutant protein. We used Western analysis to evaluate steady-state mitofusin protein levels and *Mfn2* sub-cellular localization in Control and CMT2A patient-derived fibroblasts harboring five different mutations in the *Mfn2* protein (Fig. 1). Four of the point mutations are located in the GTPase domain while the fifth is a newly identified mutation located in the HR2 region of *Mfn2*. A functional GTPase is required for an unknown step in the fusion reaction (Eura et al., 2003, Ishihara et al., 2004), while HR2 is proposed to tether adjacent organelles by forming homo- and heteromeric *Mfn1* and *Mfn2* fusion complexes (Koshiba et al., 2004, Rojo et al., 2002).

Steady-state levels of *Mfn2* protein (normalized to porin) were similar in total cell extracts from the Control and from all CMT2A fibroblast samples (Fig. 2A), indicating that *Mfn2* abundance is not affected by the presence of the mutations. Because none of the mutant *Mfn2* proteins contain amino acid substitutions in the region used to generate the antibody (a.a. 557–576), the antibody should recognize both WT and mutant *Mfn2* proteins. Similar studies using an anti-*Mfn1* antibody on the same extracts indicated that *Mfn1* protein is readily detected in human fibroblast extracts and that the presence of mutant *Mfn2* protein in CMT2A fibroblasts did not alter steady-state levels of *Mfn1* (Fig. 2A).

To determine whether the mutations being studied interfere with the targeting of the *Mfn2* protein to mitochondria, cell extracts were separated into mitochondrial (Mito) and cytoplasmic (post-mitochondrial supernatant or PMS) fractions by differential centrifugation. Each fraction was analyzed for the presence of *Mfn2* by immuno-decoration with *Mfn2* antibody as well as with antibodies to the outer mitochondrial membrane protein, porin, and the cytoplasmic protein, GAPDH (Fig. 2B). *Mfn2* protein was enriched in mitochondrial fractions and scarcely detectable in cytoplasmic fractions of both Control and CMT2A patient samples. Together, these analyses indicate that the disease-causing mutations do not change the steady-state abundance of *Mfn2* protein nor interfere with the proper targeting of *Mfn2* to mitochondria, and must instead lead to loss-of-function or dominant-negative effects.

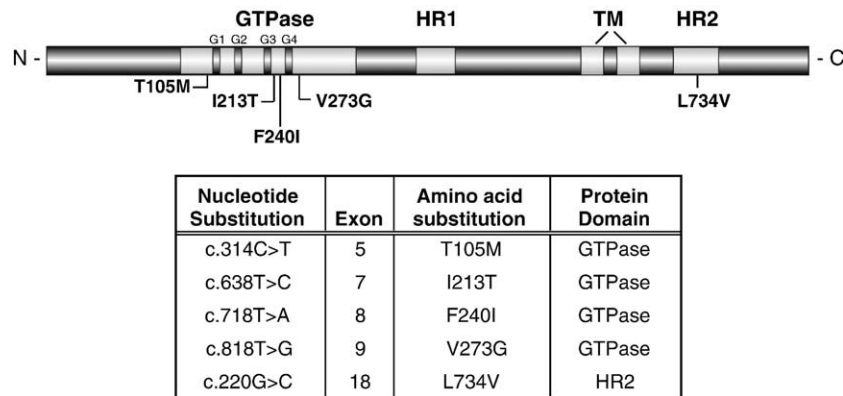


Fig. 1. Mfn2 domain structure and location of CMT2A mutations. A schematic of the predicted functional and structural domains of Mfn2. The location of each CMT2A-associated amino acid substitution analyzed in this study is indicated. G1–G4=functional motifs within the GTPase domain, TM=transmembrane domain, HR=heptad repeat or putative coiled-coil domain.

366 *Mitochondrial morphology and ultrastructure is normal in*  
367 *CMT2A patient-derived fibroblasts*

368 In most cell types, including fibroblasts, mitochondria form a  
369 distinctive network of tubules dispersed throughout the cytosol.  
370 This network is maintained by a tightly regulated balance  
371 between mitochondrial fusion and division events (reviewed by  
372 (Chan, 2006b, Chen and Chan, 2004, Okamoto and Shaw,  
373 2005). Mitochondrial fusion proteins are also involved in main-  
374 taining the distinctive cristae of the mitochondrial inner mem-

brane (Frezza et al., 2006, Griparic et al., 2004, Olichon et al., 375  
2003). We determined the effect of CMT2A-associated *MFN2* 376  
mutations on mitochondrial morphology, distribution, and 377  
membrane ultrastructure as a first indication of the ability of 378  
patient-derived fibroblasts to maintain a normal level of mito- 379  
chondrial fusion. 380

Mid-passage Control and CMT2A patient fibroblasts were 381  
stained with MitoTracker<sup>®</sup> Red CM-H<sub>2</sub>XRos (MitoTracker) and 382  
mitochondria in live cells were visualized by fluorescence 383  
microscopy (Chen et al., 2003). Mitochondrial morphology was 384

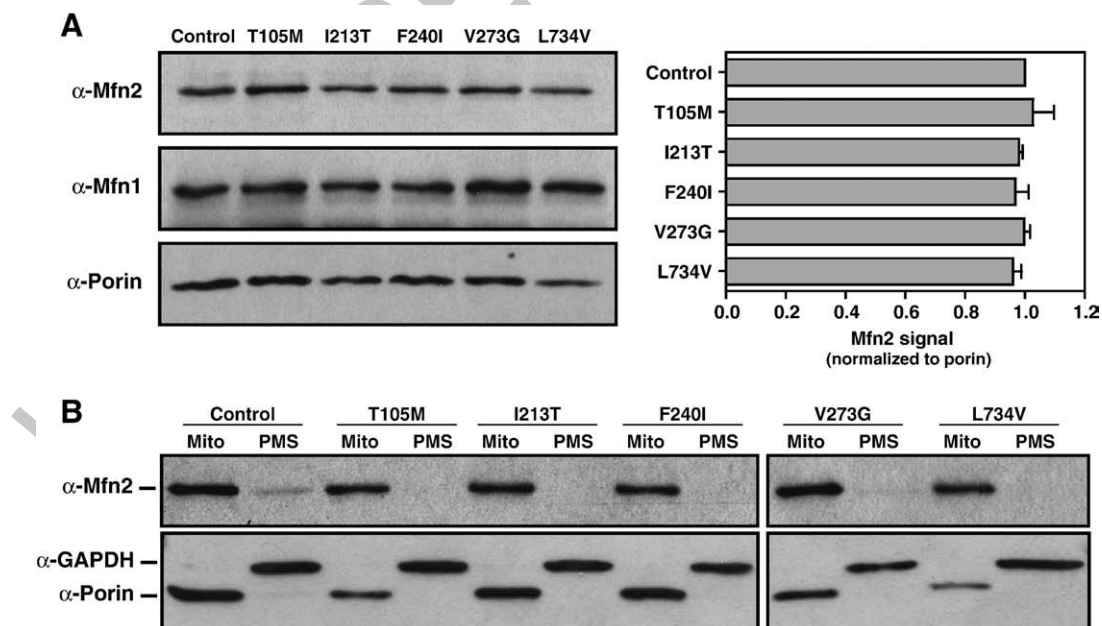


Fig. 2. Western analysis of mitofusin abundance and Mfn2 localization. (A) Western blot analysis of the mitochondrial proteins Mfn2, porin, and Mfn1 (~86 kDa, 31 kDa, and 84 kDa, respectively) in 10  $\mu$ g protein from whole cell extracts of Control and CMT2A patient-derived fibroblasts. Mfn2 signal was normalized to porin and the ratio for the Control was set equal to 1.0. Bars represent average Mfn2 levels relative to porin and error bars indicate the standard deviation from triplicate analyses. (B) Western blot analysis of Mfn2, porin, and GAPDH (~37 kDa) in mitochondrial pellets (Mito) and post-mitochondrial supernatants (PMS) from Control and Mfn2-mutant CMT2A fibroblasts. The outer mitochondrial membrane proteins Mfn2 and porin are detected primarily in the mitochondrial fractions while cytoplasmic GAPDH is only in PMS fractions. Mfn2 levels appear consistent between samples and both WT and mutant proteins are properly targeted and localized to the mitochondrial fraction.

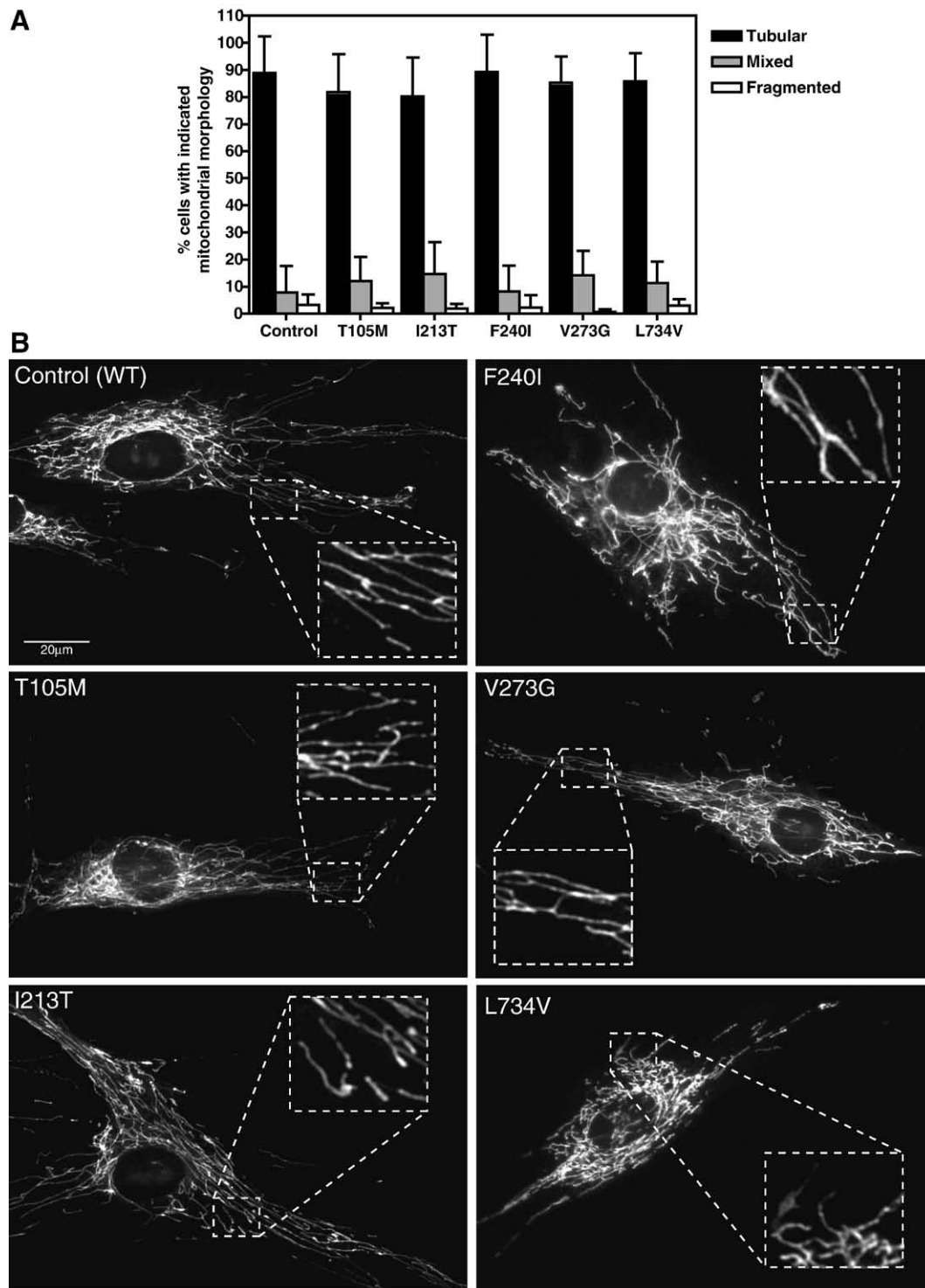


Fig. 3. Mitochondrial morphology in Control and CMT2A patient-derived fibroblasts. Primary fibroblast cultures were stained with 15nM MitoTracker for 6–8 h and visualized by fluorescence microscopy. (A) Quantification of the percent of each population exhibiting the indicated mitochondrial morphologies. Tubular=interconnected tubular mitochondrial structures forming a network distributed throughout the cell. Mixed=a combination of normal tubular structures intermixed with spherical mitochondrial fragments. Fragmented=completely fragmented or spherical mitochondria. At least 100 individual cells per population were scored per experiment. Bars represent the mean percentage per category and error bars indicate the standard deviation from triplicate experiments. (B) Representative images of MitoTracker stained mitochondria in Control and CMT2A fibroblasts with the indicated Mfn2 amino acid substitutions. Insets are zoomed to highlight distinct tubular structures in the boxed areas.

385 scored (Fig. 3A) and representative MitoTracker images of  
 386 Control and CMT2A patient fibroblasts with the indicated Mfn2  
 387 mutations are shown (Fig. 3B). No differences in mitochondrial

morphology or distribution were observed between Control and  
 388 patient fibroblasts. Electron microscopic examination further  
 389 confirmed that mitochondria in CMT2A patient fibroblasts  
 390

391 exhibit normal cytoplasmic distribution, morphology, and  
 392 ultrastructure, including the characteristic double membrane  
 393 and involuted inner membrane cristae (Fig. 4).

394 *Mitochondrial DNA integrity is normal in CMT2A*  
 395 *patient-derived fibroblasts*

396 A number of well-characterized clinical syndromes are  
 397 associated with altered mitochondrial DNA integrity or copy  
 398 number. These include large-scale single deletions in Kearns–

Sayre Syndrome (KSS), multiple deletions in dominantly 399  
 inherited chronic progressive ophthalmoplegia (CPEO), and 400  
 mitochondrial depletion syndrome due to mutations in several 401  
 of the autosomal genes responsible for mitochondrial replica- 402  
 tion or synthesis (Copeland, 2007). Disruption of mtDNA often 403  
 alters the respiratory activity of cells, which can contribute to 404  
 disease pathology. To evaluate the integrity of the mitochondrial 405  
 genome in CMT2A patient fibroblasts, a long-range PCR assay 406  
 was used to determine whether these cells contain mtDNA 407  
 rearrangements similar to those found in patients with KSS and 408

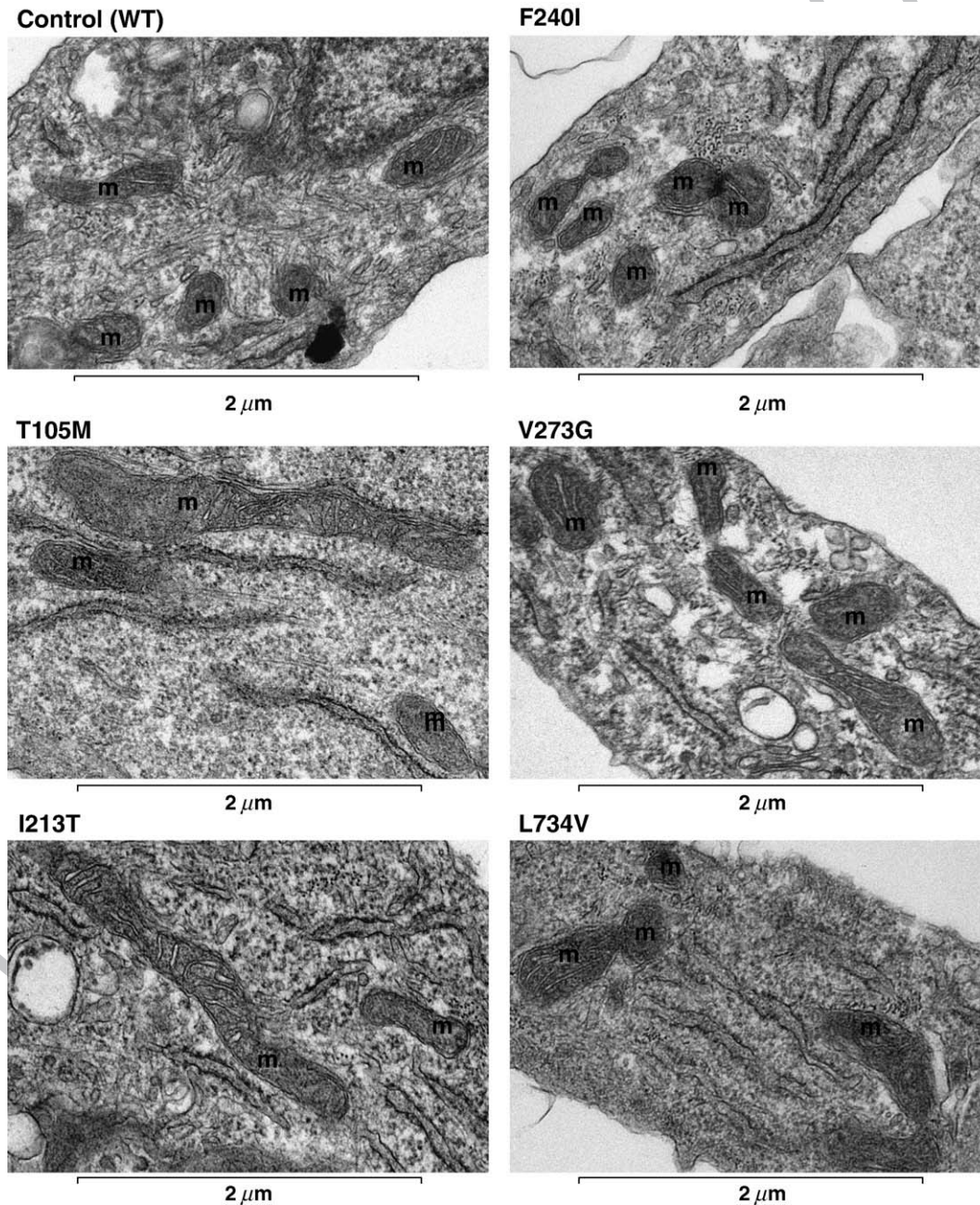
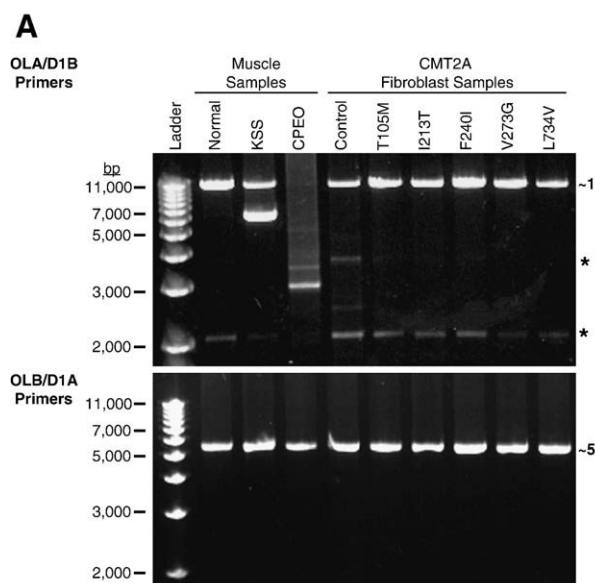


Fig. 4. Mitochondrial ultrastructure in Control and CMT2A patient-derived fibroblasts. Primary fibroblast cultures were fixed and processed for transmission electron microscopy as described in Materials and methods. Representative electron micrographs show normal gross mitochondrial morphology, quantity, and distribution in Control and the indicated Mfn2 mutant cells. Mitochondria are marked (m) and appear spherical or as longer tubules depending on the sectioning. A visible double membrane surrounds most of the pictured mitochondria and several have visible inner membrane cristae in the plane of focus, confirming normal mitochondrial ultrastructure.

409 CPEO (Kleinle et al., 1997). PCR amplification of Normal  
 410 muscle and Control fibroblast samples yielded major products  
 411 of ~11 kb and ~5.6 kb with the OLA/D1B and OLB/D1A  
 412 primers, respectively (Fig. 5A). Together these primers amplify  
 413 the entire mitochondrial genome and the products shown in the  
 414 controls indicate intact, full-length genomic mtDNA. In  
 415 contrast, OLA/D1B amplification of DNA from a KSS patient  
 416 generated a distinct ~6 kb deletion product and amplification of  
 417 the CPEO patient template produced a smear with minor bands,  
 418 indicative of multiple mtDNA deletions. Amplification of  
 419 mtDNA isolated from each of the CMT2A patient-derived  
 420 fibroblasts produced the same 11 kb and 5.6 kb products seen in  
 421 the control samples, suggesting that the CMT2A-associated



**B**

	mtDNA/ $\beta$ -globin		
	Ratio	SD	p value
Control (WT)	0.941	$\pm 0.225$	
T105M	1.109	$\pm 0.092$	0.147
I213T	1.113	$\pm 0.038$	0.130
F240I	1.249	$\pm 0.061$	0.042
V273G	0.891	$\pm 0.101$	0.373
L734V	0.891	$\pm 0.09$	0.370
All Mutants	1.051	$\pm 0.169$	0.159

Fig. 5. PCR-based mitochondrial DNA analysis. (A) Agarose gels displaying PCR products from muscle and fibroblast DNA samples using primers OLA/D1B and OLB/D1A. An 11 kb PCR product generated from OLA/D1B primers is clearly visible in “Normal” muscle and all fibroblast samples. Amplification of DNA isolated from muscle of a KSS patient produced a full-length product of 11 kb as well as a deletion product of ~6 kb. Amplification of DNA from muscle of a CPEO patient generated a large smear of DNA, indicating multiple deletions of the genome. All products generated from primers OLB/D1A are ~5.6 kb, the expected size for intact mtDNA. Asterisks (\*) indicate non-specific amplification products visible in all lanes upon longer exposure. Analysis of DNA isolated from P5 fibroblasts produced results that were identical to those shown here for P11 cells. (B) Results of qRT-PCR analysis of mtDNA in Control and CMT2A fibroblasts. The ratio of mtDNA/ $\beta$ -globin ( $\pm$ standard deviation) was calculated from triplicate experiments to determine the amount of mtDNA relative to a single copy nuclear gene ( $\beta$ -globin) in each sample. The Student’s *t*-test (unpaired, two-sample equal variance) was applied to the Control (WT) and each *MFN2* mutant sample as well as all the mutant samples pooled together (All Mutants). A *p* value  $\leq 0.05$  indicates statistical significance.

*MFN2* mutations under study do not cause instability of the 422  
 mitochondrial genome. Since mtDNA instability could increase 423  
 with progressive cell culture (particularly in the event of 424  
 defective respiration and increased reactive oxygen species 425  
 (ROS) production), we performed these assays on DNA from 426  
 primary fibroblast cultures from progressive passages (P5, not 427  
 shown, and P11, Fig. 5A). Similar results were observed with 428  
 both the P5 and P11 samples. 429

Quantitative real-time PCR (qRT-PCR) was used to compare 430  
 mtDNA content (approximate copy #) in Control and patient 431  
 samples. The quantity of both  $\beta$ -globin, a single-copy nuclear 432  
 gene, and mtDNA was calculated for each reaction based on the 433  
 standard curve (Ct versus log input DNA) generated with each 434  
 primer set (see Supplemental Table 1). The ratio of mtDNA to 435  
 $\beta$ -globin was calculated to determine the relative quantity of 436  
 mtDNA in Control and CMT2A patient cells (Fig. 5B). Relative 437  
 mtDNA levels were not statistically different from the Control 438  
 except for the F240I mutant sample (~25% more mtDNA, 439  
 $p=0.042$  by Student’s *t*-test). This subtle difference, which 440  
 probably falls within the normal range of variability in mtDNA 441  
 content, is likely unrelated to the *MFN2* mutation. It is note- 442  
 worthy that while reduced mtDNA levels have been reported in 443  
 fibroblasts from DOA patients (*OPA1* mutations) (Kim et al., 444  
 2005), the mtDNA levels measured in this collection of CMT2A 445  
 patient fibroblasts varied both above and below that of the 446  
 Control sample. When all patient samples were pooled (as done 447  
 in the DOA fibroblast study), there was no significant difference 448  
 between Control and patient mtDNA/ $\beta$ -globin ratios (Fig. 5B, 449  
 All Mutants), arguing against mtDNA loss or gain associated 450  
 with *MFN2* mutations. 451

*Respiration rates and respiratory enzyme activities are normal* 452  
*in CMT2A patient-derived fibroblasts* 453

To determine if CMT2A patient cells exhibit respiratory 454  
 defects, we measured basal and maximal (DNP-uncoupled) 455  
 rates of oxygen consumption (respiration rates) for three 456  
 CMT2A patient fibroblast cultures (Fig. 6). The vertical scatter 457  
 plots of basal (Fig. 6B) and uncoupled (Fig. 6C) measurements 458  
 from replicate experiments are included to demonstrate the 459  
 range of respiratory rates measured from the same cell culture 460  
 (including the Control). This variability resembles the range of 461  
 respiration rates measured in fibroblasts from different healthy 462  
 individuals of similar age (Greco et al., 2003) and should be 463  
 considered when trying to establish significant differences in 464  
 respiratory capacity between individuals. We found that both 465  
 mean basal and uncoupled respiration rates of CMT2A patient- 466  
 derived fibroblasts were similar to those of the Control culture 467  
 (Fig. 6A–C). Likewise, the approximately 3-fold increase in 468  
 uncoupled respiration over basal rates (Fig. 6A) for each of the 469  
 CMT2A patient-derived cultures is consistent with the ratio 470  
 observed in Control cells, suggesting that the electrochemical 471  
 gradient across the inner mitochondrial membrane is intact (no 472  
 ion leaking) and oxidative coupling is normal. 473

To confirm that the similar rates of respiration were indicative 474  
 of a properly functioning respiratory chain, we also measured 475  
 respiratory complex enzyme activities (Table 1). Consistent with 476

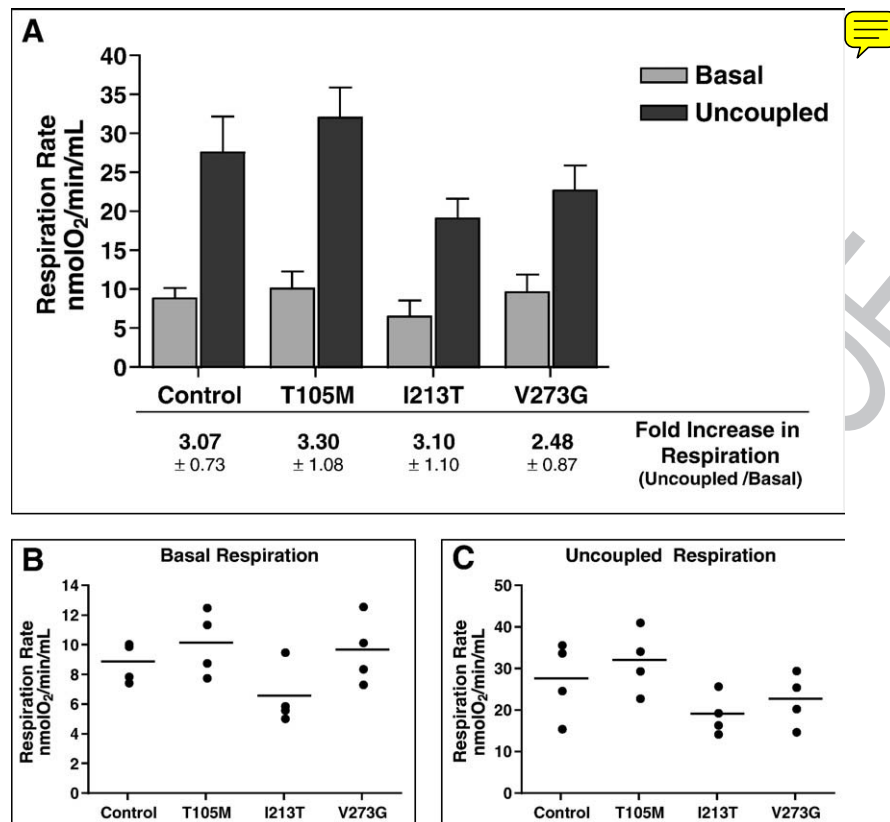


Fig. 6. Respiration rates in control and CMT2A patient-derived fibroblasts. (A) Comparison of oxygen consumption rates for Control and mutant *MFN2* (T105M, I213T, and V273G) fibroblast cultures measured under basal and uncoupled conditions. Bars represent the mean respiration rate (nmol O<sub>2</sub>/min/mL) and error bars indicate the standard deviation from four independent measurements. Listed below each set of bars is the fold increase in respiration observed upon uncoupling by DNP addition (ratio of uncoupled/basal) ± standard deviation. (B) Vertical scatter plot indicating the range of basal respiration rates observed from multiple measures for each fibroblast population. (C) Vertical scatter plot indicating the range of uncoupled respiration rates observed from multiple measures for each fibroblast population. Each circle indicates an individual data point and the horizontal bar represents the mean value from replicate measures.

477 the similarity in respiration rates, the respiratory complex  
478 enzyme activities measured in CMT2A patient-derived cul-  
479 tures did not significantly differ from those measured in Control  
480 cells.

#### 481 *Mitochondrial fusion occurs extensively in CMT2A* 482 *patient-derived fibroblasts*

483 Mitochondrial membrane fusion has been established as the  
484 primary function for Mfn2. Mouse knockout studies have  
485 shown that disruption of *MFN2* impairs the ability of  
486 mitochondria to fuse, resulting in predominantly fragmented  
487 mitochondria (Chen et al., 2005, Chen et al., 2003). However,

mitochondrial fusion has not been evaluated in human CMT2A 488  
cells, which express both WT and mutant Mfn2 proteins. 489  
Although tubular mitochondrial networks, like those observed 490  
in Fig. 3, typically indicate normal fusion activity, in 491  
*S. cerevisiae*, tubular networks are retained in the absence of 492  
fusion if division is also impaired (Sesaki and Jensen, 1999). 493  
This observation raised the possibility that tubular mitochondria 494  
could be maintained under certain conditions even in the 495  
absence of productive fusion. 496

To directly assess mitochondrial fusion competence in 497  
CMT2A patient fibroblasts, we employed a polyethylene glycol 498  
(PEG)-mediated fusion assay (Chen et al., 2003, Mattenberger 499  
et al., 2003). Cells harboring the same mutant *MFN2* allele and 500

t1.1 Table 1

t1.2 Respiratory complex enzyme activity

t1.3		NADH Dehydrogenase (I)	Succinate Dehydrogenase (II)	NADH-Cyt C Reductase (I and III)	Succinate-Cyt C Reductase (II and III)	Cytochrome C Oxidase (IV)
t1.4	Control (WT)	15	0.80	1.70	0.53	1.20
t1.5	T105M	21	1.00	2.10	0.54	1.23
t1.6	I213T	20	0.93	1.90	0.50	1.29
t1.7	V273G	19	0.62	1.90	0.37	1.06

t1.8 The enzymatic activity of respiratory complexes I–IV (as indicated) were determined and normalized to the mitochondrial content of the sample by correcting each value to CS activity (Citrate Synthase — a reference matrix enzyme). Units for the activity listed in each column are nmol/min/mg protein.

501 expressing either matrix-targeted GFP (mito-GFP) or dsRed2  
 502 (mito-RFP) were co-cultured and cell fusion was induced by  
 503 treatment with PEG. Cellular fusion is followed by cytoplasmic  
 504 mixing, which allows mito-GFP and mito-RFP labeled organelles  
 505 to interact and undergo fusion. Mixing of the fluorescent  
 506 matrix contents indicates efficient mitochondrial double  
 507 membrane fusion. Approximately 9 h after inducing cell fusion,  
 508 the resulting bi- or multi-nucleated cell hybrids were examined  
 509 for the presence of mitochondria with overlapping, or co-  
 510 localized, fluorescent red and green signal (Fig. 7, yellow  
 511 mitochondria in merged panels). Similar to the Control sample,  
 512 extensive fusion of mitochondrial tubules was observed in cell  
 513 hybrids from each of the five CMT2A patient fibroblast  
 514 cultures. Cell hybrids (both Control and patient-derived) with  
 515 mostly tubular mitochondria often contained a few discrete  
 516 spherical mitochondrial structures (fragments) that remained  
 517 unfused (see asterisks (green) and arrowheads (red); Figs. 7A'  
 518 and 7B'). We also routinely observed fused (yellow) spherical  
 519 mitochondria, indicating that the fragments were either capable  
 520 of fusion or had been generated from tubules that had fused  
 521 prior to fragmentation (arrows; Figs. 7B, B'). Because we did  
 522 not observe cell hybrids with predominantly unfused or partially

fused mitochondria, we conclude that extensive mitochondrial 523  
 fusion occurred in both Control and CMT2A patient fibroblasts. 524

## Discussion 525

One puzzling aspect of CMT2A is that the symptoms of the 526  
 disease are restricted to very specific tissues or cell types, 527  
 despite the fact that mutant *MFN2* alleles are expressed in every 528  
 cell. Thus, in addition to discovering the molecular defects 529  
 caused by *MFN2* mutations, it will be essential to uncover the 530  
 basis for the selective effects of the mutations in peripheral 531  
 nerves. While animal models will be useful for deciphering 532  
 some features of CMT2A pathogenesis, it is also necessary to 533  
 study mitochondrial function in affected and unaffected cells 534  
 from patients. Here, we have expanded upon a recent study of 535  
 CMT2A fibroblasts by evaluating mitochondrial phenotypes, 536  
 including direct assays of mitochondrial fusion and mitofusin 537  
 protein abundance, in patient fibroblasts harboring five *MFN2* 538  
 mutations not examined previously. We found that, regardless 539  
 of the location of the *Mfn2* mutation, CMT2A fibroblasts are as 540  
 robust as Control cells, with normal mitochondrial fusion and 541  
 function. Below, we summarize current molecular models for 542

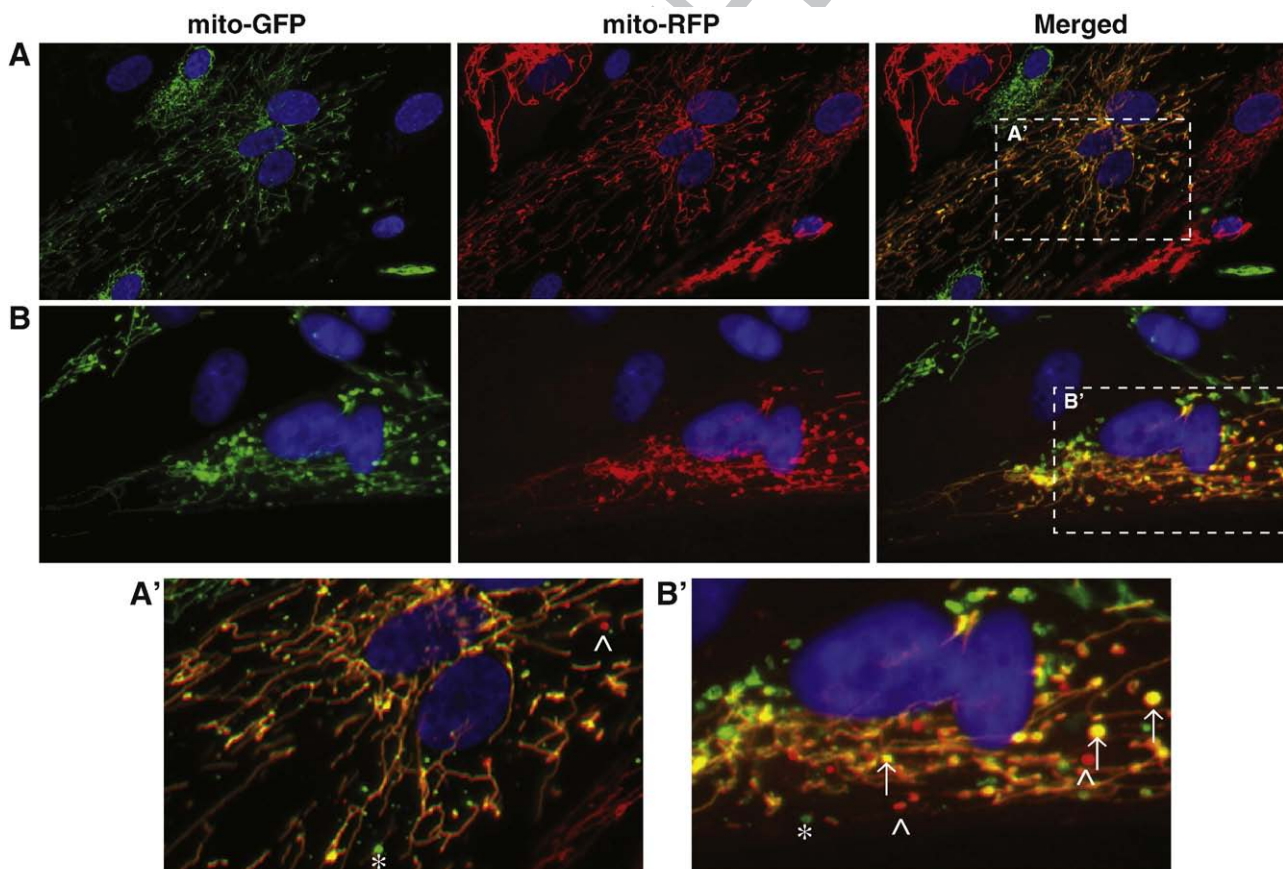


Fig. 7. Mitochondrial fusion in cell hybrids formed from Control or CMT2A patient-derived fibroblasts. PEG fusion of Control (A) and I213T mutant (B) fibroblasts expressing mito-GFP and mito-RFP. Cell hybrids contain two or more nuclei visualized with DAPI (blue) and overlapping red and green fluorescence (yellow) indicates successful mitochondrial fusion. The Control cell hybrid in (A) has normal tubular mitochondrial morphology with extensive mitochondrial fusion. The cell hybrid of I213T mutant cells in (B) displays mixed mitochondrial morphology (tubular and spherical mitochondria) with fused tubular mitochondria and some fused spherical mitochondria. (A') and (B') are zoomed images of the boxed regions in the "Merged" panels of (A) and (B), respectively. Asterisks (\*) indicate unfused mito-GFP spherical mitochondria, carets (^) indicate unfused mito-RFP spherical mitochondria, and arrows (↑) point to fused spherical mitochondria.

543 CMT2A pathology based on studies in cell cultures, mouse  
544 models, and patient-derived cells. We discuss our data in the  
545 context of these earlier findings and propose a unifying model  
546 that incorporates all available data.

547 The polarity and length of peripheral nerve axons has led to  
548 speculation that axonal degeneration in CMT2A results from  
549 failure to deliver functional mitochondria to nerve terminals. To  
550 test whether mutant Mfn2 proteins interfere with mitochondrial  
551 transport in axons, Baloh and colleagues overexpressed  
552 CMT2A alleles in primary rat DRG cells (Baloh et al., 2007).  
553 Axonal mitochondria in WT cells were simple tubules and  
554 fragments of variable length. In cells over expressing the mutant  
555 Mfn2 proteins, mitochondria were clustered in the cell body and  
556 very few organelles were seen in the axons. Based on these  
557 results, the authors proposed that mutant Mfn2 proteins interfere  
558 with an undefined role of Mfn2 in mitochondrial transport,  
559 which helps direct mitochondria down the long axons of  
560 peripheral nerves. However, interpretation of these studies is  
561 difficult because phenotypes were generated by overexpression  
562 of mutant Mfn2 protein in the presence of endogenous WT  
563 mitofusins. Overexpression of both WT and mutant Mfn2 (as  
564 well as other mitochondrial membrane proteins) has been  
565 shown to cause morphological changes (typically mitochondrial  
566 aggregation or clustering), often in a dose-dependent manner  
567 (Detmer and Chan, 2007a, Eura et al., 2003, Huang et al., 2007,  
568 Kimura and Okano, 2007, Rojo et al., 2002, Stojanovski et al.,  
569 2004, Yano et al., 1997). Since expression levels of the mutant  
570 Mfn2 proteins were not documented in the Baloh et al. study, it  
571 is difficult to predict how substantial mitochondrial aggregation  
572 and transport defects might be in neurons expressing endogen-  
573 ous levels of the mutant Mfn2 protein. In addition, mitochon-  
574 drial accumulation and impaired movement prevented direct  
575 analysis of mitochondrial fusion. Thus, the investigators could  
576 not determine whether mutant Mfn2 proteins directly impaired  
577 mitochondrial transport ~~defect~~ or whether defective movement  
578 was a secondary consequence of a change in fusion activity. Our  
579 findings that both mitochondrial fusion and distribution are  
580 normal in CMT2A patient fibroblasts (no mitochondrial  
581 clustering) would suggest that Mfn2 protein-related transport  
582 defects may be specific to neurons.

583 Another study directly tested the fusion function of CMT2A  
584 mutant Mfn2 proteins in the presence and absence of other  
585 mitofusins (Detmer and Chan, 2007a). Using this approach, the  
586 authors established that the majority of the mutant Mfn2  
587 proteins (including the T105M mutant protein analyzed here)  
588 were non-functional for fusion when expressed alone or in the  
589 presence of WT Mfn2. However, when the mutant proteins were  
590 expressed together with Mfn1, both tubular mitochondrial  
591 morphology and normal fusion activity were restored, suggest-  
592 ing that fusion competent complexes were formed between  
593 Mfn1 and mutant Mfn2. The finding that Mfn1 can correct the  
594 fusion defect of mutant Mfn2 proteins suggested a model for the  
595 tissue-specificity of the disease. As proposed by Chan and  
596 colleagues, peripheral nerves may be specifically affected in  
597 CMT2A patients because they express low levels of Mfn1 (or  
598 no Mfn1) and rely primarily on Mfn2 for fusion. By contrast,  
599 mitochondrial fusion should be normal in cells that express

Mfn1 at levels sufficient to compensate for the Mfn2 defect 600  
(Detmer and Chan, 2007a, Detmer and Chan, 2007b). Con- 601  
sistent with this model, we found that CMT2A patient fibro- 602  
blasts express Mfn1, and that mitochondria in these cells fuse 603  
normally. In principle, siRNA knockdown of Mfn1 could be 604  
used to reveal fusion defects associated with the Mfn2 muta- 605  
tions in CMT2A patient fibroblasts. However, the results of 606  
such studies would be difficult or impossible to interpret due to 607  
mitochondrial fusion deficiencies and fragmentation caused by 608  
Mfn1 knockdown alone (Eura et al., 2003). Ultimately, vali- 609  
dation of this model will require analysis of Mfn1 and Mfn2 610  
expression levels in a collection of human tissues with an 611  
emphasis on the affected neuronal cell types. 612

613 Although the creation of a mouse model for CMT2A would  
614 greatly facilitate studies of disease pathology and tissue-  
615 specificity, initial studies indicate that mice heterozygous for a  
616 common CMT2A allele (*MFN2*<sup>+R94Q</sup>) do not exhibit neurologi-  
617 cal phenotypes (Detmer and Chan, 2007a). In addition, 617  
conditional Mfn2 knockout mice experience neurodegeneration 618  
and exhibit mitochondrial abnormalities in Purkinje cells, but 619  
the mouse phenotype does not mimic CMT2A disease (Chen 620  
et al., 2007). Finally, a transgenic mouse expressing the T105M 621  
*MFN2* mutation directly in motor neurons was recently de- 622  
scribed (Detmer et al., 2007). These mice display axonal loss, 623  
muscle atrophy, and hind-limb gait defects resembling CMT2A, 624  
however, the phenotype could only be generated upon 625  
significant overexpression of the transgene. Together, these 626  
observations suggest that development of a CMT2A mouse 627  
model may not be straightforward, and emphasize the impor- 628  
tance of carrying out future studies in human stem-cell derived 629  
or primary neuronal cultures as well as in CMT2A patient cells 630  
and tissues. 631

632 Prior to our study, mitochondrial function had only been  
633 examined in CMT2A fibroblasts carrying three of the  
634 approximately 40 known *MFN2* lesions (Loiseau et al., 2007).  
635 This study, like ours, reported essentially normal mitochondrial  
636 morphology, mtDNA content, respiration rates, and respiratory  
637 complex activity in patient fibroblasts. In addition, the authors  
638 found no significant differences in ATP production, ROS  
639 generation, or susceptibility to apoptosis-inducing agents.  
640 However, they did report statistically significant increases in  
641 oligomycin-insensitive respiration as well as decreases in  
642 mitochondrial membrane potential ( $\Delta\Psi$ ) and mitochondrial  
643 coupling efficiency ([ATP]/oxygen consumed). These results  
644 are surprising because respiratory chain dysfunction is often  
645 associated with altered mitochondrial morphology, mtDNA  
646 integrity, and defects in electron transport components. In  
647 addition, the severity of the reported coupling defects is not  
648 consistent with the clinical severity of patient symptoms. The  
649 authors speculated that CMT2A symptoms may result from  
650 neuronal sensitivity to these subtle changes in mitochondrial  
651 energetics (Loiseau et al., 2007), however, it is not yet clear  
652 whether the coupling defects reported by Loiseau et al. are a  
653 direct consequence of the *MFN2* mutations or whether these  
654 defects do in fact contribute to CMT2A pathology. 654

655 While no single model discussed above fully explains the  
656 published data, the combined results can be accommodated by a 656

657 synthesis of all the models. Specifically, the data suggest that  
 658 fibroblasts and other unaffected CMT2A patient cells express  
 659 sufficient levels of Mfn1 to allow the formation of functional  
 660 fusion complexes that maintain mitochondrial integrity. In  
 661 contrast, peripheral nerves are more sensitive to the presence of  
 662 mutant Mfn2 proteins due to low levels of Mfn1 (Detmer and  
 663 Chan, 2007a, Detmer and Chan, 2007b). The formation of  
 664 mostly non-functional Mfn2–Mfn2<sup>mutant</sup> fusion complexes  
 665 (Detmer and Chan, 2007a) in an environment with little to no  
 666 Mfn1 would reduce the frequency of efficient fusion and may  
 667 generate an energetically heterogeneous population of mito-  
 668 chondria in the affected cells (Chen et al., 2005, Loiseau et al.,  
 669 2007). It has been shown that axonal transport of mitochondria  
 670 depends on mitochondrial function, such that energetically  
 671 compromised mitochondria are preferentially transported from  
 672 the synapse back to the cell body (Miller and Sheetz, 2004). As  
 673 a result, mitochondria are in short supply at the nerve terminal  
 674 where they are needed to provide energy essential for synaptic  
 675 function (Verstreken et al., 2005). Alternatively, axonal  
 676 transport defects could arise from mitochondrial aggregation  
 677 (Baloh et al., 2007, Detmer and Chan, 2007a), perhaps caused  
 678 by mutant fusion complexes that prolong, or make permanent,  
 679 the tethering of adjacent mitochondria (Eura et al., 2003, Huang  
 680 et al., 2007, Koshiba et al., 2004, Rojo et al., 2002). In either  
 681 case, depletion of mitochondria from peripheral nerve axons  
 682 and terminals could cause progressive degeneration of these  
 683 structures, producing the CMT2A symptoms observed in the  
 684 patients. If this cascade of cellular events can be experimentally  
 685 validated, it is possible that up-regulation of *MFN1* expression  
 686 or delivery of Mfn1 protein to peripheral nerves (Detmer and  
 687 Chan, 2007a) might slow or block the progression of clinical  
 688 symptoms in individuals diagnosed with CMT2A.

## 689 Acknowledgments

690 We gratefully acknowledge Ling Zhao for her technical  
 691 assistance in performing mtDNA deletion analyses; the  
 692 University of Utah School of Medicine Cell Imaging Facility  
 693 for confocal microscope use and imaging assistance; the  
 694 Genomics Core Facility of the University of Utah for qRT-  
 695 PCR advising and equipment use; Ms Michelle Husain for her  
 696 excellent EM technical expertise; Charles Murtaugh for use of  
 697 his IX71 fluorescence microscope; Manuel Rojo for Mfn1  
 698 antibody; Dean Tantin for cell culture facilities, supplies, and  
 699 advice; Richard Cawthon for discussion on mtDNA quantifica-  
 700 tion; and David Chan and Hsiuchen Chen for providing  
 701 protocols and technical advice. Most importantly, we are  
 702 grateful to the CMT2A patients and their families for their  
 703 valuable personal contributions to our studies. This research  
 704 was supported by: NRSA T32 Institutional Training Grant (HD  
 705 07576-22) to EAA; National Center for Research Resources  
 706 (1S10RR023454-01) to JMM; NINDS (K08 NS 48180) to  
 707 PBK; NIH Mentored Research Development Award  
 708 (SK23NS42713-05) and University of Utah Research Founda-  
 709 tion seed grant to VHL; NIH (GM 53466) to JMS; and the  
 710 National Center for Research Resources (M01-RR00064) to the  
 711 University of Utah (L. Betz, P.I.).

## Appendix A. Supplementary data

712

Supplementary data associated with this article can be found,  
 713 in the online version, at doi:10.1016/j.expneurol.2008.01.010. 714

## References

715

- Baloh, R.H., 2007. Mitochondrial dynamics and peripheral neuropathy. *Neuroscientist*. 716  
717
- Baloh, R.H., Schmidt, R.E., Pestronk, A., Milbrandt, J., 2007. Altered axonal  
718 mitochondrial transport in the pathogenesis of Charcot–Marie–Tooth  
719 disease from mitofusin 2 mutations. *J. Neurosci.* 27, 422–430. 720
- Baxter, R.V., Ben Othmane, K., Rochelle, J.M., Stajich, J.E., Hulette, C., Dew-  
721 Knight, S., Hentati, F., Ben Hamida, M., Bel, S., Stenger, J.E., Gilbert, J.R.,  
722 Pericak-Vance, M.A., Vance, J.M., 2002. Ganglioside-induced differentia-  
723 tion-associated protein-1 is mutant in Charcot–Marie–Tooth disease type  
724 4A/8q21. *Nat. Genet.* 30, 21–22. 725
- Cawthon, R.M., 2002. Telomere measurement by quantitative PCR. *Nucleic*  
726 *Acids Res.* 30, e47. 727
- Chan, D.C., 2006a. Mitochondria: dynamic organelles in disease, aging, and  
728 development. *Cell* 125, 1241–1252. 729
- Chan, D.C., 2006b. Mitochondrial fusion and fission in mammals. *Annu. Rev.*  
730 *Cell Dev. Biol.* 22, 79–99. 731
- Chan, D.C., 2007. Mitochondrial dynamics in disease. *N. Engl. J. Med.* 356,  
732 1707–1709. 733
- Chen, H., Chan, D.C., 2004. Mitochondrial dynamics in mammals. *Curr. Top.*  
734 *Dev. Biol.* 59, 119–144. 735
- Chen, H., Chan, D.C., 2006. Critical dependence of neurons on mitochondrial  
736 dynamics. *Curr. Opin. Cell Biol.* 18, 453–459. 737
- Chen, H., Detmer, S.A., Ewald, A.J., Griffin, E.E., Fraser, S.E., Chan, D.C.,  
738 2003. Mitofusins Mfn1 and Mfn2 coordinately regulate mitochondrial  
739 fusion and are essential for embryonic development. *J. Cell Biol.* 160,  
740 189–200. 741
- Chen, H., Chomyn, A., Chan, D.C., 2005. Disruption of fusion results in  
742 mitochondrial heterogeneity and dysfunction. *J. Biol. Chem.* 280,  
743 26185–26192. 744
- Chen, H., McCaffery, J.M., Chan, D.C., 2007. Mitochondrial fusion protects  
745 against neurodegeneration in the cerebellum. *Cell* 130, 548–562. 746
- Chung, K.W., Kim, S.B., Park, K.D., Choi, K.G., Lee, J.H., Eun, H.W., Suh, J.S.,  
747 Hwang, J.H., Kim, W.K., Seo, B.C., Kim, S.H., Son, I.H., Kim, S.M.,  
748 Sunwoo, I.N., Choi, B.O., 2006. Early onset severe and late-onset mild  
749 Charcot–Marie–Tooth disease with mitofusin 2 (MFN2) mutations. *Brain*  
750 129, 2103–2118. 751
- Copeland, W.C., 2007. Inherited mitochondrial diseases of DNA replication.  
752 *Annu. Rev. Med.* 753
- Cuesta, A., Pedrola, L., Sevilla, T., Garcia-Planells, J., Chumillas, M.J.,  
754 Mayordomo, F., LeGuern, E., Marin, I., Vilchez, J.J., Palau, F., 2002. The  
755 gene encoding ganglioside-induced differentiation-associated protein 1 is  
756 mutated in axonal Charcot–Marie–Tooth type 4A disease. *Nat. Genet.* 30,  
757 22–25. 758
- Delettre, C., Lenaers, G., Griffioen, J.M., Gigarel, N., Lorenzo, C., Belenguer, P.,  
759 Pelloquin, L., Grosgeorge, J., Turc-Carel, C., Perret, E., Astarie-Dequeker,  
760 C., Lasquellce, L., Arnaud, B., Ducommun, B., Kaplan, J., Hamel, C.P.,  
761 2000. Nuclear gene OPA1, encoding a mitochondrial dynamin-related  
762 protein, is mutated in dominant optic atrophy. *Nat. Genet.* 26, 207–210. 763
- Detmer, S.A., Chan, D.C., 2007a. Complementation between mouse Mfn1 and  
764 Mfn2 protects mitochondrial fusion defects caused by CMT2A disease  
765 mutations. *J. Cell Biol.* 176, 405–414. 766
- Detmer, S.A., Chan, D.C., 2007b. Functions and dysfunctions of mitochondrial  
767 dynamics. *Nat. Rev. Mol. Cell Biol.* 8, 870–879. 768
- Detmer, S.A., Velde, C.V., Cleveland, D.W., Chan, D.C., 2007. Hindlimb gait  
769 defects due to motor axon loss and reduced distal muscles in a transgenic  
770 mouse model of Charcot–Marie–Tooth type 2A. *Hum. Mol. Genet.* 771
- DiMauro, S., Servidei, S., Zeviani, M., DiRocco, M., DeVivo, D.C., DiDonato,  
772 S., Uziel, G., Berry, K., Hoganson, G., Johnsen, S.D., et al., 1987. 773  
774 Cytochrome *c* oxidase deficiency in Leigh syndrome. *Ann. Neurol.* 22,  
775 498–506. 775

- 776 Eura, Y., Ishihara, N., Yokota, S., Mihara, K., 2003. Two mitofusin proteins,  
777 mammalian homologues of FZO, with distinct functions are both required  
778 for mitochondrial fusion. *J. Biochem. (Tokyo)* 134, 333–344.
- 779 Frezza, C., Cipolat, S., Martins de Brito, O., Micaroni, M., Beznoussenko, G.V.,  
780 Rudka, T., Bartoli, D., Polishuck, R.S., Danial, N.N., De Strooper, B.,  
781 Scorrano, L., 2006. OPA1 controls apoptotic cristae remodeling independ-  
782 dently from mitochondrial fusion. *Cell* 126, 177–189.
- 783 Greco, M., Villani, G., Mazzucchelli, F., Bresolin, N., Papa, S., Attardi, G.,  
784 2003. Marked aging-related decline in efficiency of oxidative phosphoryla-  
785 tion in human skin fibroblasts. *Faseb J.* 17, 1706–1708.
- 786 Griparic, L., van der Wel, N.N., Orozco, I.J., Peters, P.J., van der Blik, A.M.,  
787 2004. Loss of the intermembrane space protein Mgm1/OPA1 induces  
788 swelling and localized constrictions along the lengths of mitochondria.  
789 *J. Biol. Chem.* 279, 18792–18798.
- 790 Higuchi, R., Fockler, C., Dollinger, G., Watson, R., 1993. Kinetic PCR analysis:  
791 real-time monitoring of DNA amplification reactions. *Biotechnology (N Y)*  
792 11, 1026–1030.
- 793 Huang, P., Yu, T., Yoon, Y., 2007. Mitochondrial clustering induced by  
794 overexpression of the mitochondrial fusion protein Mfn2 causes mitochon-  
795 drial dysfunction and cell death. *Eur. J. Cell Biol.* 86, 289–302.
- 796 Ishihara, N., Eura, Y., Mihara, K., 2004. Mitofusin 1 and 2 play distinct roles in  
797 mitochondrial fusion reactions via GTPase activity. *J. Cell Sci.* 117, 6535–6546.
- 798 Kijima, K., Numakura, C., Izumino, H., Umetsu, K., Nezu, A., Shiiki, T.,  
799 Ogawa, M., Ishizaki, Y., Kitamura, T., Shozawa, Y., Hayasaka, K., 2005.  
800 Mitochondrial GTPase mitofusin 2 mutation in Charcot–Marie–Tooth  
801 neuropathy type 2A. *Hum. Genet.* 116, 23–27.
- 802 Kim, J.Y., Hwang, J.M., Ko, H.S., Seong, M.W., Park, B.J., Park, S.S., 2005.  
803 Mitochondrial DNA content is decreased in autosomal dominant optic  
804 atrophy. *Neurology* 64, 966–972.
- 805 Kimura, M., Okano, Y., 2007. Human Misato regulates mitochondrial  
806 distribution and morphology. *Exp. Cell Res.* 313, 1393–1404.
- 807 Kleinle, S., Wiesmann, U., Superti-Furga, A., Krahenbuhl, S., Boltshauser, E.,  
808 Reichen, J., Liechti-Gallati, S., 1997. Detection and characterization of  
809 mitochondrial DNA rearrangements in Pearson and Kearns–Sayre syn-  
810 dromes by long PCR. *Hum. Genet.* 100, 643–650.
- 811 Koshiba, T., Detmer, S.A., Kaiser, J.T., Chen, H., McCaffery, J.M., Chan, D.C.,  
812 2004. Structural basis of mitochondrial tethering by mitofusin complexes.  
813 *Science* 305, 858–862.
- 814 Lawson, V.H., Graham, B.V., Flanigan, K.M., 2005. Clinical and electro-  
815 physiologic features of CMT2A with mutations in the mitofusin 2 gene.  
816 *Neurology* 65, 197–204.
- 817 Legros, F., Lombes, A., Frachon, P., Rojo, M., 2002. Mitochondrial fusion in  
818 human cells is efficient, requires the inner membrane potential, and is  
819 mediated by mitofusins. *Mol. Biol. Cell* 13, 4343–4354.
- 820 Loiseau, D., Chevrollier, A., Verny, C., Guillet, V., Gueguen, N., Pou de  
821 Crescenzo, M.A., Ferre, M., Malinge, M.C., Guichet, A., Nicolas, G.,  
822 Amati-Bonneau, P., Malthiery, Y., Bonneau, D., Reynier, P., 2007.  
823 Mitochondrial coupling defect in Charcot–Marie–Tooth type 2A disease.  
824 *Ann. Neurol.* 61, 315–323.
- 825 Mattenberger, Y., James, D.I., Martinou, J.C., 2003. Fusion of mitochondria in  
826 mammalian cells is dependent on the mitochondrial inner membrane  
827 potential and independent of microtubules or actin. *FEBS Lett.* 538, 53–59.
- 828 McCaffery, J.M., Farquhar, M.G., 1995. Localization of GTPases by indirect  
829 immunofluorescence and immunoelectron microscopy. *Methods Enzymol.*  
830 257, 259–279.
- 831 Miller, K.E., Sheetz, M.P., 2004. Axonal mitochondrial transport and potential  
832 are correlated. *J. Cell Sci.* 117, 2791–2804.
- 833 Niemann, A., Ruegg, M., La Padula, V., Schenone, A., Suter, U., 2005.  
834 Ganglioside-induced differentiation associated protein 1 is a regulator of the  
894 mitochondrial network: new implications for Charcot–Marie–Tooth disease. *J. Cell Biol.* 170, 1067–1078. 836
- O'Neill, B.T., Kim, J., Wende, A.R., Theobald, H.A., Tuinei, J., Buchanan, J., 837  
Guo, A., Zaha, V.G., Davis, D.K., Schell, J.C., Boudina, S., Wayment, B., 838  
Litwin, S.E., Shioi, T., Izumo, S., Birnbaum, M.J., Abel, E.D., 2007. A 839  
conserved role for phosphatidylinositol 3-kinase but not Akt signaling in 840  
mitochondrial adaptations that accompany physiological cardiac hypertro- 841  
phy. *Cell Metab.* 6, 294–306. 842
- Okamoto, K., Shaw, J.M., 2005. Mitochondrial morphology and dynamics in 843  
yeast and multicellular eukaryotes. *Annu. Rev. Genet.* 39, 503–536. 844
- Olichon, A., Baricault, L., Gas, N., Guillou, E., Valette, A., Belenguer, P., 845  
Lenaers, G., 2003. Loss of OPA1 perturbs the mitochondrial inner 846  
membrane structure and integrity, leading to cytochrome *c* release and 847  
apoptosis. *J. Biol. Chem.* 278, 7743–7746. 848
- Parfait, B., Rustin, P., Munnich, A., Rotig, A., 1998. Co-amplification of nuclear 849  
pseudogenes and assessment of heteroplasmy of mitochondrial DNA 850  
mutations. *Biochem. Biophys. Res. Commun.* 247, 57–59. 851
- Rojo, M., Legros, F., Chateau, D., Lombes, A., 2002. Membrane topology and 852  
mitochondrial targeting of mitofusins, ubiquitous mammalian homologs of 853  
the transmembrane GTPase Fzo. *J. Cell. Sci.* 115, 1663–1674. 854
- Santel, A., Frank, S., Gaume, B., Herrler, M., Youle, R.J., Fuller, M.T., 2003. 855  
Mitofusin-1 protein is a generally expressed mediator of mitochondrial 856  
fusion in mammalian cells. *J. Cell Sci.* 116, 2763–2774. 857
- Sesaki, H., Jensen, R.E., 1999. Division versus fusion: Dnm1p and Fzo1p 858  
antagonistically regulate mitochondrial shape. *J. Cell Biol.* 147, 699–706. 859
- Stojanovski, D., Koutoupoulos, O.S., Okamoto, K., Ryan, M.T., 2004. Levels of 860  
human Fis1 at the mitochondrial outer membrane regulate mitochondrial 861  
morphology. *J. Cell Sci.* 117, 1201–1210. 862
- Verhoeven, K., Claeys, K.G., Zuchner, S., Schroder, J.M., Weis, J., Ceuterick, 863  
C., Jordanova, A., Nelis, E., De Vriendt, E., Van Hul, M., Seeman, P., 864  
Mazanec, R., Saifi, G.M., Szigeti, K., Mancias, P., Butler, I.J., Kochanski, 865  
A., Ryniewicz, B., De Bleeker, J., Van den Bergh, P., Verellen, C., Van 866  
Coster, R., Goemans, N., Auer-Grumbach, M., Robberecht, W., Milic Rasic, 867  
V., Nevo, Y., Tournev, I., Guergueltcheva, V., Roelens, F., Vieregge, P., 868  
Vinci, P., Moreno, M.T., Christen, H.J., Shy, M.E., Lupski, J.R., Vance, J.M., 869  
De Jonghe, P., Timmerman, V., 2006. MFN2 mutation distribution and 870  
genotype/phenotype correlation in Charcot–Marie–Tooth type 2. *Brain* 129, 871  
2093–2102. 872
- Verstreken, P., Ly, C.V., Venken, K.J., Koh, T.W., Zhou, Y., Bellen, H.J., 2005. 873  
Synaptic mitochondria are critical for mobilization of reserve pool vesicles 874  
at *Drosophila* neuromuscular junctions. *Neuron* 47, 365–378. 875
- Yano, M., Kanazawa, M., Terada, K., Namchai, C., Yamaizumi, M., Hanson, B., 876  
Hoogenraad, N., Mori, M., 1997. Visualization of mitochondrial protein 877  
import in cultured mammalian cells with green fluorescent protein and 878  
effects of overexpression of the human import receptor Tom20. *J. Biol.* 879  
*Chem.* 272, 8459–8465. 880
- Zuchner, S., De Jonghe, P., Jordanova, A., Claeys, K.G., Guergueltcheva, V., 881  
Cherninkova, S., Hamilton, S.R., Van Stavern, G., Krajewski, K.M., Stajich, 882  
J., Tournev, I., Verhoeven, K., Langerhorst, C.T., de Visser, M., Baas, F., 883  
Bird, T., Timmerman, V., Shy, M., Vance, J.M., 2006. Axonal neuropathy 884  
with optic atrophy is caused by mutations in mitofusin 2. *Ann. Neurol.* 59, 885  
276–281. 886
- Zuchner, S., Mersyanova, I.V., Muglia, M., Bissar-Tadmouri, N., Rochelle, J., 887  
Dadali, E.L., Zappia, M., Nelis, E., Patitucci, A., Senderek, J., Parman, Y., 888  
Evgrafov, O., Jonghe, P.D., Takahashi, Y., Tsuji, S., Pericak-Vance, M.A., 889  
Quattrone, A., Battaloglu, E., Polyakov, A.V., Timmerman, V., Schroder, 890  
J.M., Vance, J.M., 2004. Mutations in the mitochondrial GTPase mitofusin 891  
2 cause Charcot–Marie–Tooth neuropathy type 2A. *Nat. Genet.* 36, 892  
449–451. 893